RSC Applied Polymers

ROYAL SOCIETY OF CHEMISTRY

PAPER

View Article Online
View Journal | View Issue

Cite this: *RSC Appl. Polym.*, 2025, **3**, 1366

Optimization of light-curing ionogels by response surface methodology

Dejun Peng, [a,b] Zeyu Zhang, *[a,b] Xueyan Shang,[a,b] Jiguo Zhang[a,b] and Shixue Ren *[a,b]

Received 31st December 2024,
Accepted 6th August 2025

DOI: 10.1039/d4lp00381k

rsc.li/rscapplpolym

Because of their unique properties, ionogels are very suitable for wide application in fields such as energy storage devices and wearable devices, but poor mechanical strength limits their practical use. Polyols or compounds containing multiple unsaturated double bonds are typically used as cross-linking agents in the construction of gels, but it is difficult to balance mechanical strength with flexibility because these compounds mainly form linear or simple reticular structures. It is, therefore, important to design ionogels with improved mechanical properties. Here, response surface methodology was used to optimize the preparation of light-curing ionogels, using the biomass-derived polymer rutin as an antioxidant cross-linking agent. The prepared ionogels had a tensile strength as high as 639.15 kPa, which was attributed to the three-dimensional cross-linked network structure formed by esterified rutin and to the sacrificial hydrogen bond energy dissipation mechanism. After light curing of the esterified rutin by free radical polymerisation, the structure retained the intact conjugated system and thus provided good UV protection (light transmission in UVB region = 0%). This study offers a new way to rapidly prepare high-performance UV-resistant polymer coatings, which show promise for applications in sunscreen coatings, such as parasols and automotive/architectural sunscreen glass.

1 Introduction

Ionogels are gels made of ionic liquid as a dispersing medium, swollen by polymer networks, with a three-dimensional mesh structure formed by chemical cross-linking or physical entanglement of polymer molecular chains. Compared with other hydrogels, ionogels have high ionic conductivity, high thermal and chemical stability, good electrochemical stability and low flammability.[1–6] Because of these desirable properties, ionogels are particularly suitable for use in fields such as energy storage devices,[7–9] wearable devices[10–15] and soft robotics.[16–18]

One shortcoming of most ionogels is that they have poor mechanical properties, including low strength, poor toughness, and susceptibility to fatigue damage, all of which limit their practical applications.[19–21] The underlying cause of these poor mechanical properties is the use of polyols or compounds with multiple unsaturated double bonds as cross-linking agents in the construction of the gels. This leads to the formation of low-density polymer chains or non-homogeneous polymer networks and makes it difficult to balance mechanical strength and flexibility. Altering the mode of cross-linking of the polymer chains is considered to be one of the most effective ways of regulating macroscopic properties and thus addressing the problem of poor mechanical properties. Two main approaches have been used; the first is to toughen the ionogel by introducing non-covalent bonding and the second is to toughen the ionogel by the use of covalent polymer networks. As examples of the first approach, Yu *et al.*[22] developed hydrogels with good mechanical properties by constructing a gel system containing opposing charges and Guo *et al.*[23] developed hydrogels with good mechanical properties by exploiting Cu^{2+} coordination. In the latter case, the dissolved polyelectrolyte hydrogel was immersed in $CuSO_4$ solution, producing dynamic coordination bonds (P–Cu–O) between Cu^{2+} ions and phosphorus and oxygen atoms in the monomer, and thereby significantly increasing fracture stress (from 10.3 kPa to 570 kPa). Hydrogels toughened by non-covalent toughening agents are, however, susceptible to structural degradation brought about by environmental changes (temperature, humidity, pH, *etc.*).[24] The second approach to improving mechanical properties, toughening by covalent polymer networks, has, therefore, received increasing attention. For example, Fang *et al.*[25] prepared toughened ionogels using fibrillar connected double networks, in which a polyacrylamide network and an acrylated agarose fibril network

[a]*State Key Laboratory of Woody Oil Resources Utilization, Northeast Forestry University, Harbin 150040, China. E-mail: zhangzeyu666999@163.com, Renshixue@nefu.edu.cn*
[b]*College of Materials Science and Engineering, Northeast Forestry University, Harbin 150040, China*

were chemically cross-linked, leading to an increase in tensile strength from 2 MPa to 8 MPa.

Because of their low toxicity and high reactivity,[26–28] polyphenols derived from agroforestry-derived biomass have recently attracted much attention as precursors to hydrogels that are widely used for sustained drug release.[28] The structure of the polyhydroxyl compound is key since this provides the basis for modifications.[16,29,30] Biomass-derived polyphenols typically have a polycyclic, multibranched structure and, when used as cross-linking agents, increase the cross-linking density of the gel. Construction of a sacrificial energy dissipation network and increased cross-linking density are important ways to enhance tensile strength and toughness. A fruitful avenue of research would be the preparation of novel cross-linking agents by modification of bio-based polyphenols and regulation of the mechanical properties of ionogels by optimizing the ratio of molecular chains to cross-linkers.

In this study, photocurable ionogels (PAMG-Rs) were successfully prepared using biomass-derived esterified rutin as the cross-linking agent and acrylamide as the monomer. The numerous reaction sites of esterified rutin allowed construction of a three-dimensional mesh structure and increased the cross-linking density, giving the gel excellent tensile strength. A regression model was constructed using response surface methodology to optimize the preparation process and determine the optimal ratio of starting materials for the PAMG-Rs. Compared with light-curing ionogels that have *N*,*N*′-methylenebisacrylamide as the cross-linker and acrylamide as the monomer (PAMG-Ns), PAMG-Rs have higher tensile strength and energy dissipation, combined with good compressive properties and toughness. Fourier-transform infrared (FT-IR) spectroscopy, proton nuclear magnetic resonance (^{1}H NMR) spectroscopy, ultraviolet (UV) spectroscopy scanning electron microscopy (SEM) and X-ray diffraction (XRD) were used to investigate the mechanism of action of biomass-derived polyphenols when used as cross-linking agents in ionogels. The PAMG-Rs have excellent UV shielding properties, high transparency and good adhesion to glass, making them particularly suitable for use in sunscreen coatings, such as parasols and automotive/architectural UV-resistant glass.

2 Materials and methods

2.1 Materials

Rutin (95%), triethylamine (99%), methacryloyl chloride (95%) and 1-ethyl-3-methylimidazole acetate (97%) were purchased from Shanghai Aladdin Biochemical Science and Technology Co., Ltd (Shanghai, China); diphenyl (2,4,6-trimethylbenzoyl) phosphine oxide (97%), Darocur 2959 (2-hydroxy-4′-(2-hydroxyethoxy)-2-methylpropiophenone (98%)) and acrylamide (99%) were purchased from Macklin Biochemistry Co., Ltd (Shanghai, China); *N*,*N*-dimethylacetamide (99.5%) was purchased from Tianjin Fuyu Fine Chemical Co., Ltd (Tianjin, China); and *N*,*N*′-methylenebisacrylamide (98%) was purchased from Tianjin Guangfu Fine Chemical Research Institute (Tianjin, China). All chemicals were used as received without any further purification and deionised water was used in all experiments.

2.2 Preparation of esterified rutin

A flask containing a solution of rutin (0.6105 g) and triethylamine (2.08 mL) in *N*,*N*-dimethylacetamide (10 mL) was filled with N_2 and sealed. A constant pressure dropping funnel containing a solution of methacryloyl chloride (1.568 g) in *N*,*N*-dimethylacetamide (10 mL) was connected to the flask, filled with N_2 and sealed. The flask was placed in an ice-water bath, and the solution of methacryloyl chloride in *N*,*N*-dimethylacetamide was slowly added dropwise. The flask was then transferred to an oil bath at 25 °C, and the reaction was continued for 72 h. The resulting solution was slowly poured onto deionised water and the resulting precipitate was filtered, washed with water and dried to give esterified rutin (Fig. 1a).

2.3 Preparation of ionogels

In separate experiments, the cross-linking agents, esterified rutin (for PAMG-R ionogels) and *N*,*N*′-methylenebisacrylamide (for PAMG-N ionogels), were completely dissolved in 1-ethyl-3-methylimidazole acetate with the aid of a cell crusher. The monomer, acrylamide, and deionised water were added and the mixture was stirred to give complete dissolution. Initiator (Darocur 2959 and TPO) was then added and the mixture again stirred to give complete dissolution. The mixture was then poured into a polytetrafluoroethylene mold and cured using UV light (45 W, λ = 365 nm) to give the PAMG-R and PAMG-N ionogels (Fig. 1b).

2.4 Response surface methodology

Based on the results of the single-factor experiments, the tensile strength of the prepared ionogel was taken as the response value, and the initiator, cross-linking agent and monomer were selected as three factors. The experimental factors and their levels are shown in Table 1.

2.5 Characterization and testing of ionogels

2.5.1 Structural analysis. FT-IR spectra of the PAMG-N and PAMG-R ionogels were recorded over the range 4200–500 cm^{-1} using a Nicolet iN10 FT-IR spectrophotometer (Thermo Fisher Scientific, USA). The resolution was 4 cm^{-1} and the number of scans was 32.

SEM was carried out using an Apreo S HiVac scanning electron microscope (Thermo Fisher Scientific, USA). The freeze-dried ionogel was pasted onto the sample stage using conductive adhesive and sprayed with gold for 20 s at 5 kV. The sample was then placed in the vacuum chamber of the scanning electron microscope. The gel surface was observed under 5 kV voltage, with a standard flow beam.

XRD maps were recorded using a Panalytical X'Pert Pro X-ray diffractometer (Malvern Panalytical, Malvern, UK). Data were acquired over the range 10–80°, with a scanning speed of 10° min^{-1}.

Transparency was measured using a TU-1950 UV-vis spectrophotometer (Beijing Puxi General Instrument Co., Ltd,

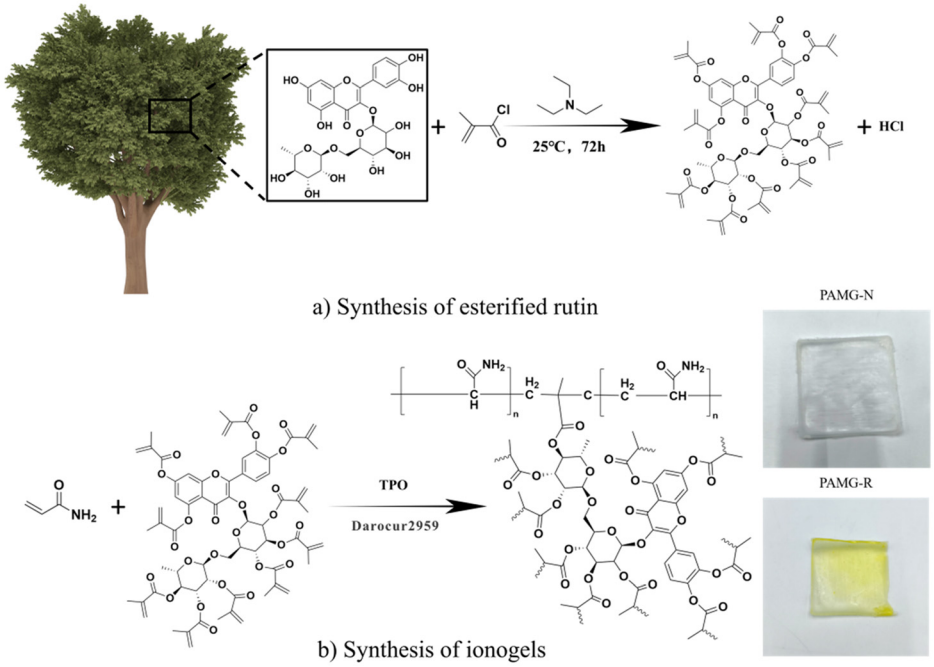

Fig. 1 Preparation of PAMG-R ionogel and digital photos of cured PAMG-N and PAMG-R ionogels (TPO, 2,4,6-trimethylbenzoyl) phosphine oxide.

Beijing, China), over the range 800–200 nm, with air as the reference.

2.5.2 Performance testing. Tensile strength and elongation at break were measured on spindle-shaped specimens of the ionogels using a UTM 2203 electronic universal testing machine (Shenzhen Suns Technology Stock Co., Ltd, Shenzhen, China).[18]

Compressive stress was measured on cylindrical specimens of the ionogels using an INSTRON 5982 electronic universal testing machine (INSTRON Test Equipment Trading Co., Ltd, Shanghai, China). Adhesive properties were measured by uniformly coating an area (25 mm × 25 mm) between two slides with the ionogel precursor, tightly pressing the slides together and irradiating under UV light for 5 min. After complete curing, the tensile strength of the ionogel was measured using a UTM2203 electronic universal testing machine at the time of separation to assess the adhesion strength of the ionogels after curing quantitatively.

2.5.3 Statistical analysis of data. Based on the results of a one-factor experiment, response surface methodology was used to carry out a three-factor, three-level response surface optimisation design. The mass fractions of initiator, cross-linking agent and monomer were used as factors and the tensile strength of the ionogel was used as the response value. Design-Expert v11.0 software was used to analyze the results according to Box-Behnken design.

Table 1 Factors and levels of experiment design

	Coded value		
Factors	−1	0	+1
A mass fraction of initiator (wt%)	2	3	4
B mass fraction of cross-linker (wt%)	0.1	0.35	0.6
C mass fraction of monomer (wt%)	36	38	40

3 Results and analyses

3.1 Box-Behnken design

3.1.1 Box-Behnken test results. To determine the factors affecting the performance of ionogels prepared by photoinitiation, tensile strength (MPa) was used as the response index (Y) and the mass fractions of initiator (A), cross-linking agent (B) and monomer (C) were used as the influencing factors. A Box-Behnken response surface test was designed to optimise the synthetic method, and the experimental results were analyzed using Design Expert v11.0 software. The experimental design and data are shown in Table 2. A quadratic multiple regression model was established for the optimal conditions for preparation of the photoinitiated ionogels, as shown in eqn (1):

$$Y = -10.87 + 0.37A + 7.43B + 0.47C - 0.051AB - 0.004181AC - 0.21BC - 0.032A^2 + 0.98B^2 - 0.004934C^2 \quad (1)$$

3.1.2 Significance of regression model. The model was statistically tested using analysis of variance (ANOVA), which is used to test the necessity and adequacy of the model (Table 3). The F-value of the model was 4.1117 (*i.e.*, >1), which indicates that the model is significant. The probability of such a large F-value due to noise is only 0.04%, with a P-value <0.0500, which also indicates that the model term is significant. The

Table 2 Box-Benkhen design with independent variables and response values

Code	Independent variable						Tensile strength (Y, MPa)	
	Mass fraction of initiator (A)		Mass fraction of cross-linker (B)		Mass fraction of monomer (C)		Actual	Predicted
1	1	4	−1	0.1	0	38	0.063676	0.132192
2	−1	2	0	0.35	1	40	0.065059	0.05797
3	0	3	1	0.6	1	40	0.032346	0.03488
4	0	3	1	0.6	−1	36	0.21298	0.208988
5	1	4	1	0.6	0	38	0.153243	0.098192
6	−1	2	1	0.6	0	38	0.176646	0.121148
7	1	4	0	0.35	−1	36	0.00465	0.024622
8	0	3	−1	0.1	1	40	0.2326	0.25338
9	0	3	−1	0.1	−1	36	0.000672	0.007488
10	0	3	0	0.35	0	38	0.059573	0.08467
11	1	4	0	0.35	1	40	0.03544	0.04379
12	0	3	0	0.35	0	38	0.15681	0.08467
13	0	3	0	0.35	0	38	0.059573	0.08467
14	0	3	0	0.35	0	38	0.059573	0.08467
15	0	3	0	0.35	0	38	0.055716	0.08467
16	−1	2	0	0.35	−1	36	0.000822	0.005354
17	−1	2	−1	0.1	0	38	0.035881	0.104148

Table 3 Analysis of variance for tensile strength model

Origin	Sum of squared deviations from mean	Degrees of freedom	Mean square	F-Value	P-Value	Significance
Model	0.0742	9	0.0082	4.1117	0.0378	Significant
A	0.0047	1	0.0047	2.3404	0.1699	
B	0.0025	1	0.0025	1.2363	0.3029	
C	0.0123	1	0.0123	6.1381	0.0424	
AB	0.0007	1	0.0007	0.3268	0.5854	
AC	0.0003	1	0.0003	0.1395	0.7198	
BC	0.0426	1	0.0426	21.2235	0.0025	
A^2	0.0043	1	0.0043	2.1535	0.1857	
B^2	0.0157	1	0.0157	7.8489	0.0265	
C^2	0.0016	1	0.0016	0.8178	0.3959	
Residual	0.0140	7	0.0020			
Lost proposal	0.0063	3	0.0021	1.0887	0.4498	Insignificant
Pure error	0.0077	4	0.0019			
Total	0.0882	16				

F-value for lack of fit was 1.0887, which implies that the lack of fit is not statistically significant relative to pure error. The adequacy of the Box-Behnken design model diagnostic plots and 3D contour response surface plots are shown in Fig. 2. The expected probability and internal study residuals are very close to the same straight line, indicating that the model is stochastic (Fig. 2a). The predicted and actual values are also close to the same straight line, demonstrating that the fit is better, and that the correlation between experimental and predicted values is very high and accurate (Fig. 2b). The residuals of the internal study for each experimental point are <4, indicating that the model is reliable (Fig. 2c).

The ANOVA of the tensile strength model is shown in Table 3. From the magnitude of the F-value of the regression model, the order of influence of each factor was determined to be: mass fraction of monomer (C) > mass fraction of initiator (A) > mass fraction of cross-linker (B). Analysis of the significance of the P-value showed that C, BC and B^2 are essential model terms ($P < 0.05$).

3.1.3 Response surface analysis. The steepness of the slope of the response surface of each factor reflects the degree of influence of that factor on the tensile strength of the ionogel; the steeper the response surface, the more significant the interaction. As shown in Fig. 2d–f, the curve for C is the steepest, indicating that the mass fraction of the monomer has the most significant effect on the maximum tensile strength of the light-curing ionogel. The mass fraction of the initiator has the second most significant effect, and the mass fraction of the cross-linking agent has a more minor impact. BC has the largest interaction, indicating that the mass fractions of the initiator and monomer significantly affect the tensile strength of the light-curing ionogel. AB has the second largest interaction, indicating that the mass fractions of the initiator and cross-linking agent have a specific effect on the tensile strength of the light-curingionogel. The AC interaction is weak, indicating that the mass fractions of the initiator and monomer have less effect on the tensile strength of light-curing ionogel.

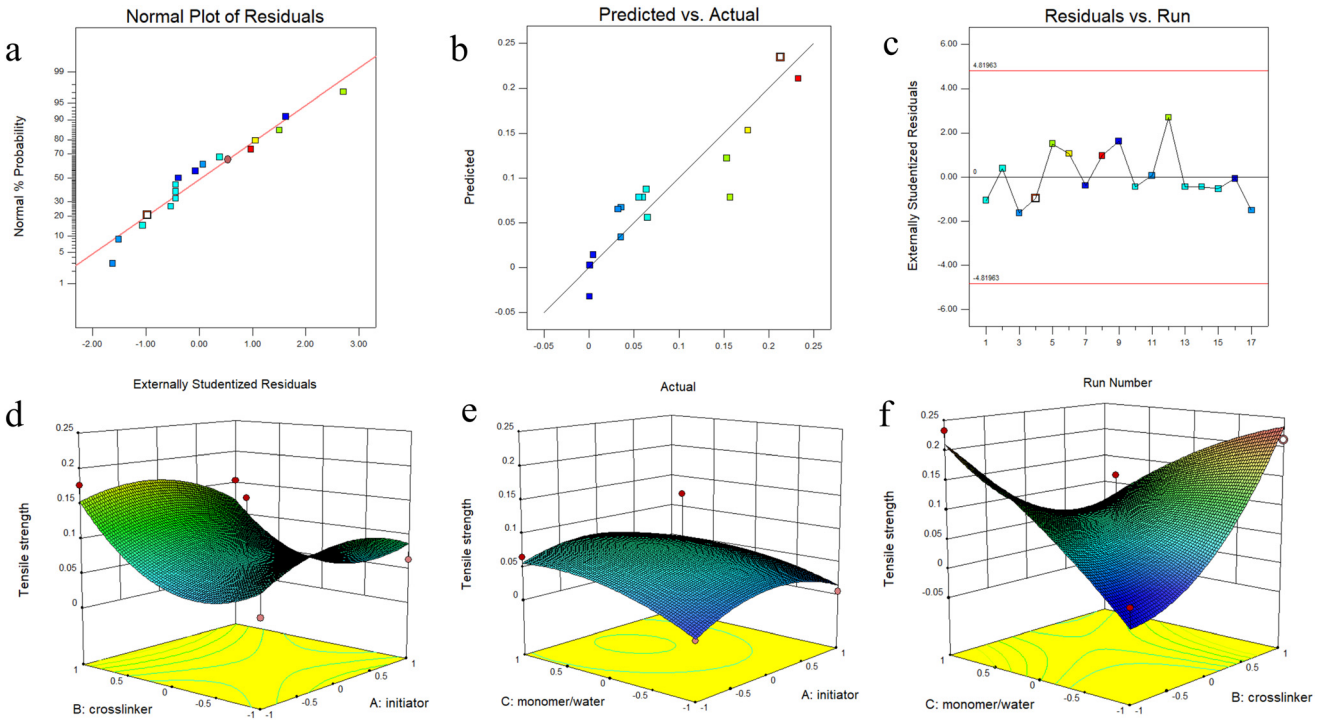

Fig. 2 Adequacy of diagnostic plots of Box-Behnken design model and response surface plots of 3D contours. (a) Normal probability plots of residuals; (b) plots of residuals *vs.* predicted; (c) plots of residuals *vs.* run; response surface plots showing (d) interaction of A *vs.* B on tensile strength; (e) interaction of A *vs.* C on tensile strength; (f) interaction of B *vs.* C on tensile strength.

Model validation experiments were carried out next to validate the model using the optimum formulation conditions obtained from response surface methodology. The experiment was conducted using mass fractions of 36.014% monomer, 0.58% cross-linker and 3.714% initiator. With these mass fractions, the tensile strength was 639.15 kPa (Fig. 5a), which is very different from the predicted value of 193 kPa. After full consideration of the experimental design and operational process, there were seen to be differences in the temperature and humidity of the experimental environment, which may affect the resultant values; the photoinitiation time also has some influence on the formation and physicochemical properties of the ionogel. Comprehensive analysis indicated that this experimental scheme has an important reference value and guiding significance. To further explore the effect of the structure of the cross-linking agent, esterified rutin, on the mechanical and adhesive properties of the ionogels, we compared the ionogels prepared using esterified rutin (PAMG-Rs) at the aforementioned optimal ratio with the ionogels prepared using *N*,*N*′-methylenebisacrylamide as the cross-linking agent at the same ratio (PAMG-Ns). All subsequent tests were carried out in accordance with this.

3.2 Design, synthesis and structural characterization

3.2.1 Structural characterization of esterified rutin. In the presence of triethylamine, the phenolic hydroxyl groups of rutin undergo a nucleophilic substitution reaction with methacryloyl chloride to produce esterified rutin.[31] Comparing the FT-IR spectra of rutin and esterified rutin (Fig. 3a), it can be clearly seen that the peak at approximately 3400 cm^{-1} in the FT-IR spectrum of rutin, attributed to telescopic vibrations of phenolic hydroxyl groups, has essentially disappeared in the FT-IR spectrum of esterified rutin. The peak at δ = 12.61 in the ^{1}H NMR spectrum of rutin had also disappeared in the ^{1}H NMR spectrum of esterified rutin. The peaks at δ = 7.53 in the ^{1}H NMR spectrum of rutin, corresponding to the hydroxyl group on the other benzene ring in rutin, and at δ = 4.53, corresponding to the hydroxyl group on the oxygen-containing cycloalkane groups in rutin, had also both essentially disappeared in the ^{1}H NMR spectrum of esterified rutin. In the FT-IR spectrum of esterified rutin, a new peak at approximately 1750 cm^{-1} corresponds to telescopic vibrations of ester (–COO–) groups and, in the ^{1}H NMR spectrum, a new peak at δ = 3.34 represents the methyl group of the methacryl moiety, confirming the successful preparation of esterified rutin.

3.2.2 Structural characterization of ionogels. Ionogels were prepared using acrylamide as the monomer and esterified rutin as the cross-linking agent to increase the cross-linking density, and a polyacrylamide molecular chain was used as the molecular backbone. The FT-IR spectra of PAMG-N and PAMG-R were very similar (Fig. 4a), with peaks on both sides of 3250 cm^{-1} attributed to antisymmetric stretching vibrations of primary amide groups (–$CONH_2$) in the cross-linked structure. This indicates that the two ionogels have the same cross-linked backbone structure and confirms the successful preparation of the polymers. In the ^{1}H NMR spectra (Fig. 4b), the

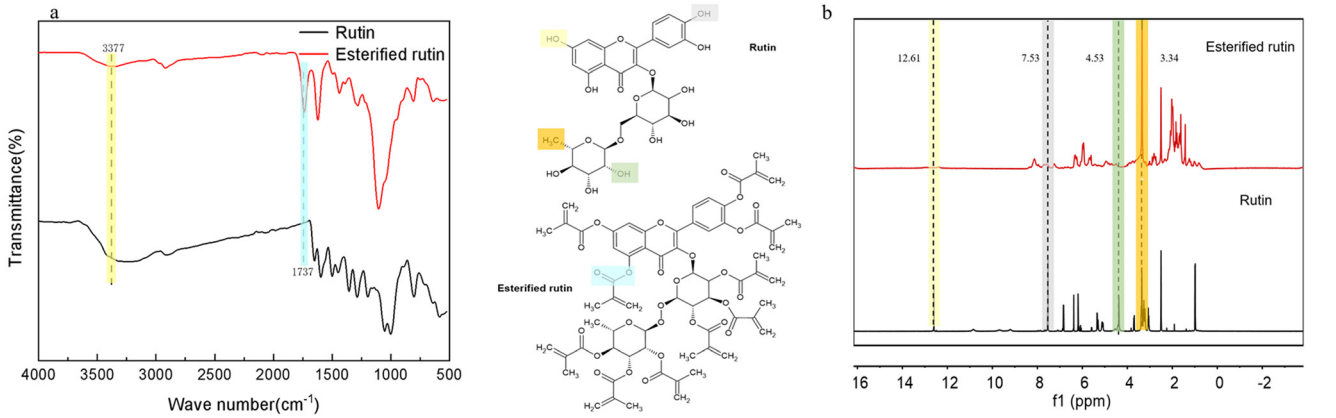

Fig. 3 Structural characterization of rutin and esterified rutin. (a) FT-IR spectra of rutin and esterified rutin; (b) ^{1}H NMR spectra of rutin and esterified rutin.

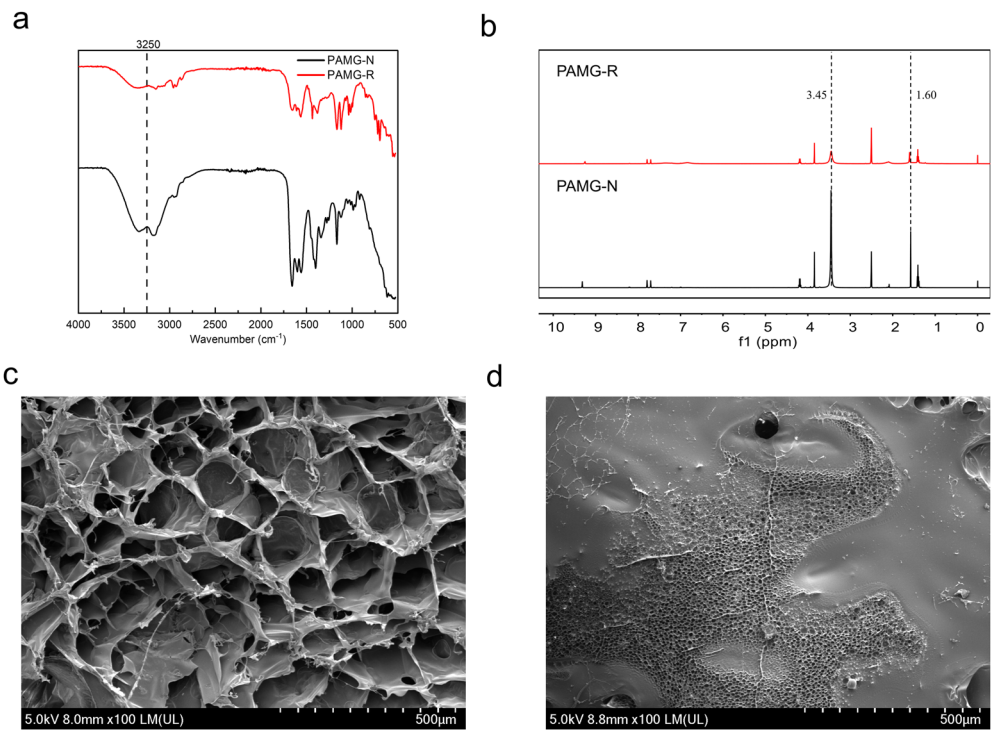

Fig. 4 Structural characterization of PAMG-N and PAMG-R. (a) FT-IR spectra of PAMG-N and PAMG-R; (b) ^{1}H NMR spectra of PAMG-N and PAMG-R; (c) SEM image of PAMG-N; (d) SEM image of PAMG-R.

secondary amide group (–C(═O)NH–) of PAMG-N cross-linker at δ = 3.45, and both peaks existed near δ = 1.6, considered the primary amide group of acrylamide.

The SEM images of PAMG-N and PAMG-R (Fig. 4c and d, respectively) both show uneven surfaces, with a large number of distributed pores that provide space for energy dissipation at the macroscopic level and allow the possibility of adsorption and piggybacking of functional particles. Increasing the cross-linking density decreases the porosity; the pore structure of PAMG-R is denser, and the cavity density is greater, than that of PAMG-N, providing a structural basis for better energy dissipation in PAMG-R.[32]

In the swelling test (Fig. S1), PAMG-R absorbed water rapidly and swelled by more than 200% within 5 minutes. In sharp contrast, PAMG-N swelled slowly and swelled by only 50% after 5 minutes; PAMG-N needed 10 hours to swell by 200%. After 1 hour, PAMG-R had formed a semi-solid visco-elastic colloid with slow, self-supporting flow characteristics. This indirectly demonstrates that the cross-linking density of PAMG-R is greater than that of PAMG-N.

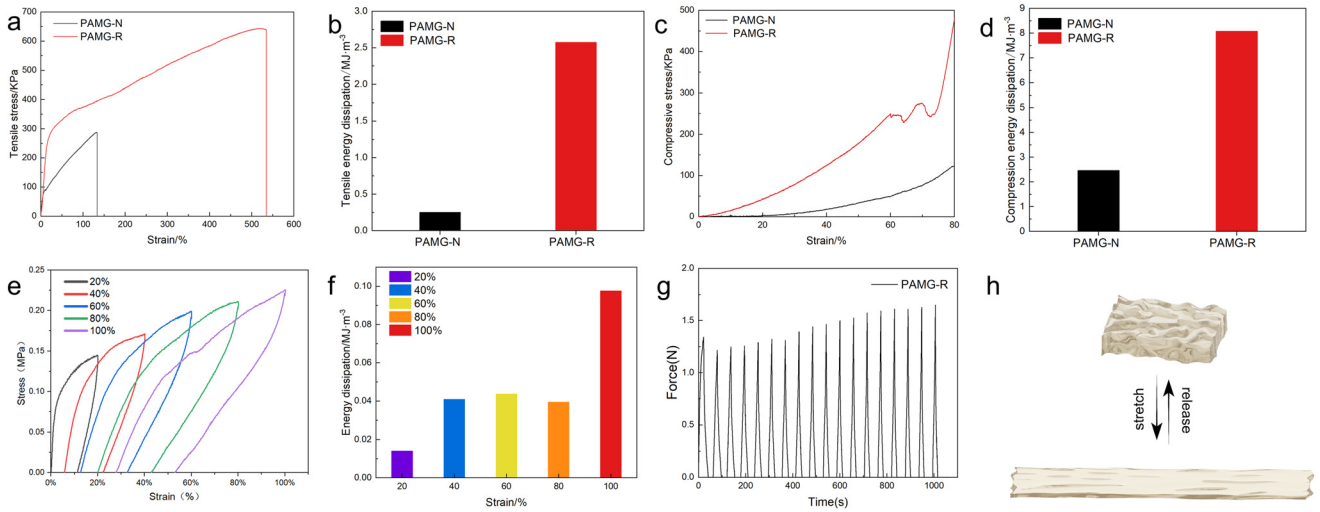

Fig. 5 Characterization of mechanical properties of PAMG-N and PAMG-R. (a) The tensile stress–strain curves of PAMG-R and PAMG-N; (b) The tensile toughness of PAMG-R and PAMG-N; (c) The compressive stress–strain curves of PAMG-R and PAMG-N; (d) The compressive toughness of PAMG-R and PAMG-N; (e) The cyclic loading and unloading tensile curves generated by PAMG-R under strains of 20%, 40%, 60%, 80%, and 100%. (f) Energy dissipation of PAMG-R at strains of 20%, 40%, 60%, 80% and 100%. (g) Tensile force variation curves 18 cycles of loading and unloading at 50% fixed strain. (h) The schematic diagram of the stretch and release of PAMG-R.

3.3 Mechanical properties of ionogels

The tensile stress–strain curves and toughness of PAMG-R and PAMG-N are shown in Fig. 5a and b, respectively. The tensile stress of PAMG-R (639.15 kPa) was 223% that of PAMG-N and the toughness of PAMG-R was approximately 10-fold higher than that of PAMG-N. This indicates that physical entanglement of the polyacrylamide molecular chains (hydrogen bonding, van der Waals forces, *etc.*) is disrupted during stretching. In the second half of the stress–strain curve, however, the PAMG-R stress–strain is increasing, indicating that the esterified rutin cross-linking agent increases the cross-linking density of the whole system. The ionic liquids and linear polymer molecular chains simultaneously form hydrogen bonds between the dissipation of energy. It will play a molecular chain of the effect of the 'physical lubricant' to simultaneously ensure the dynamics of the polymer network. The ionic liquids act as 'physical lubricants' between the molecular chains, providing the dynamics of the polymer network and simultaneously giving structural stability, and thus improving the tensile strength and toughness of PAMG-R.

The breaking of bonds leads to energy dissipation[33] and the PAMG-R ionogel system is rich in hydrogen bonds. van der Waals forces, which are the first to break when the ionogel is stretched, release more energy to combat deformation,[34,35] and the gel system sacrifices hydrogen bonding to reduce damage to the polyacrylamide molecular chain. This high level of energy dissipation enhances the toughness of the ionogel.

The compressive stress–strain curves and compressive toughness of PAMG-R and PAMG-N are shown in Fig. 5c and d, respectively. When the compression ratio is 40%, the compressive stress of PAMG-R (124 kPa) is higher than that of PAMG-N (18 kPa), when the compression ratio is 60%, the compressive stress of PAMG-R (248 kPa) remains higher than that of PAMG-N (49 kPa), and when the compression ratio is 80%, the compressive stress of PAMG-R (472 kPa) is also higher than that of PAMG-N (123 kPa). The compressive stress of PAMG-R is thus significantly higher than that of PAMG-N in all test intervals. When the compressive deformation is 80%, the compressive toughness of PAMG-R is more than 300% that of PAMG-N. This demonstrates that PAMG-R has greater toughness than PAMG-N when compressed by an external force and undergoes effective deformation and accumulates more energy than PAMG-N. This is due to the denser and more stable mesh structure of PAMG-R, which gives it better compressive strength and compressive toughness.

To investigate the ability of PAMG-R to recover, cyclic loading and unloading tensile curves were generated under strains of 20%, 40%, 60%, 80%, and 100% at the same rate (Fig. 5e). The stress of PAMG-R increased rapidly under increasing strain and, as the strain increased further, the stress decreased slowly, producing a hysteresis curve. As the tension increases, hydrogen bonds between the ionic liquid and the polyacrylamide molecular chain are broken to dissipate energy and these bonds are reformed when the stress is released, although the cross-linked network of covalent bonds remains intact (Fig. 5f).

Over 18 cycles of stretch-unloading at 50% strain, the strain increased slowly with the number of cycles (Fig. 5g). Cyclic hardening occurred, which was attributed to the presence of numerous reactive sites in the cross-linked network of PAMG-R, which can form new non-covalent interactions under continuous loading-unloading, as set out in the intrinsic model proposed by You *et al.*[36] In this model, the tensile stresses produced during stretching of PAMG-R cause orientation of the molecular chains and thus improve the mechanical strength of PAMG-R. Ionogels are viscoelastic materials and

the viscous component leads to stress relaxation, creep during stretching and unloading, and the phenomenon of hysteresis. Hysteresis also occurs because of the non-covalent interactions, such as hydrogen bonding and van der Waals forces, in PAMG-R, which are destroyed during stretching and re-formed during unloading, leading to energy dissipation.

3.4 UV shielding properties of ionogels

The XRD diffraction curves of PAMG-N and PAMG-R are shown in Fig. 6a. Both PAMG-N and PAMG-R show significant broad dispersion peaks around 20°, indicating that the polymers have an amorphous structure. The amorphous polymer chain segments are irregularly stacked and the disordered structure means that the gel state is homogeneous and the polymers are, therefore, transparent. Good transparency extends the range of applications of an ionogel but generally leads to poor UV shielding. The good light transmittance of PAMG-N and PAMG-R can be clearly seen in Fig. 6d.

Prolonged exposure to the UVB region of the spectrum (280–320 nm), which is widely acknowledged to cause photocoagulation and suppress the function of the immune system, is the main cause of non-melanoma skin cancer. Prolonged exposure to the UVA region of the spectrum (320–400 nm) can cause skin aging, pigmentation and indirect damage to DNA. As shown in Fig. 6b, PAMG-R provides much better shielding than PAMG-N over the wavelength range 320–400 nm. The transmittance of 320 nm and 400 nm light by PAMG-R was 0% and 64.3%, respectively. PAMG-R can thus effectively absorb and reflect UV light while allowing the longer wavelengths of visible light to pass through, indicating excellent UV shielding. This is because the conjugated structure of rutin, which has intrinsic UV-shielding properties (Fig. S2), is retained in the PAMG-R ionogel after preparation of the cross-linking agent by esterification of rutin. During formation of the gel, a larger area of p–π conjugation is also formed. Because of the electronic transition effect, this leads to greater absorption of UV light and enhances UV shielding. Materials that have a large number of intermolecular interactions, such as hydrogen bonds, which affect UV penetration, have enhanced UV shielding properties.[37] Our results show that PAMG-R has excellent UV-blocking properties and high transparency and can thus safely protect skin and adherent surfaces from solar irradiation and photoaging.[38]

To demonstrate the UV shielding properties of PAMG-R, we applied an anti-counterfeiting mark to a 100-yuan RMB note. When viewed under 365 nm UV light, the anti-counterfeiting mark on the uncovered 100-yuan note was very obvious (Fig. 6e (I)) and the anti-counterfeiting mark covered by PAMG-N was

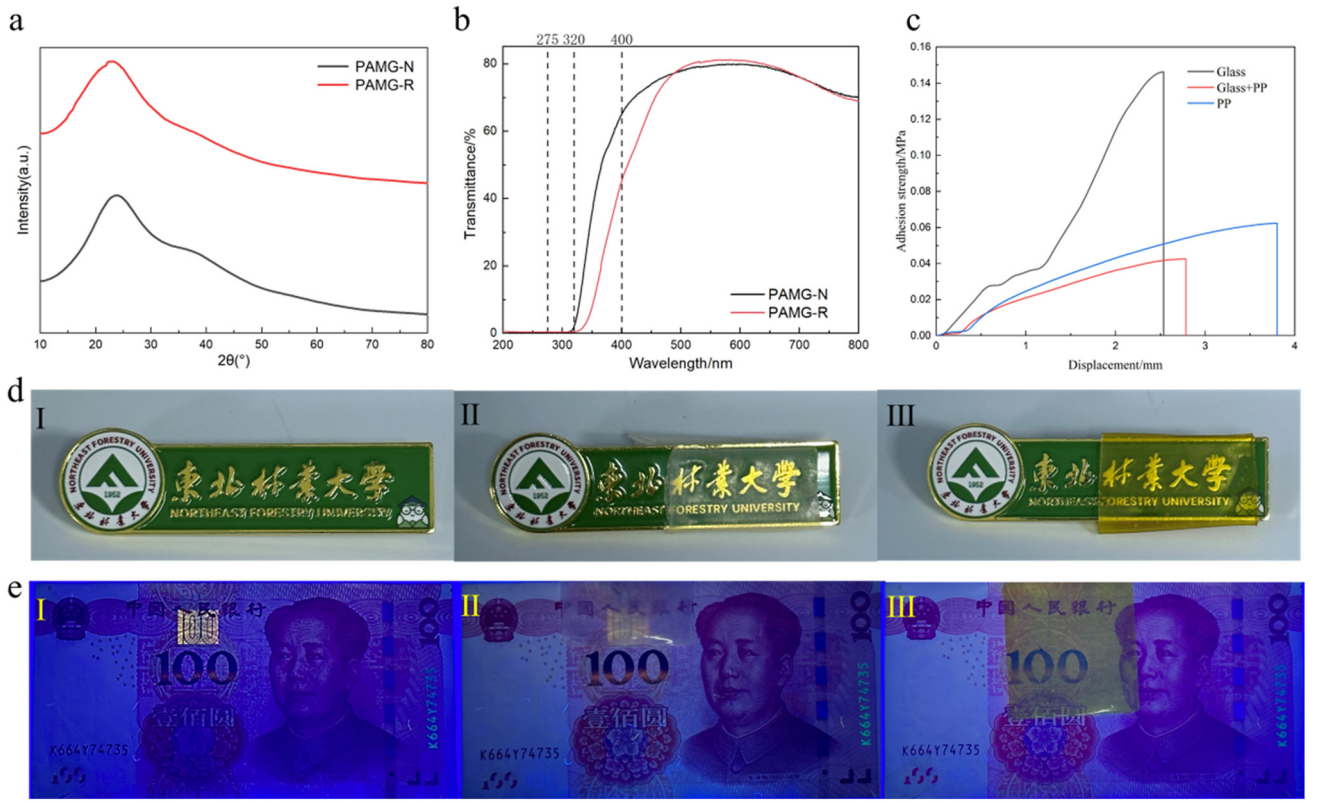

Fig. 6 UV shielding and adhesive performance of ionogels. (a) XRD spectra of PAMG-R and PAMG-N; (b) UV transmittance curves of PAMG-R and PAMG-N; (c) adhesive strength-displacement curve of PAMG-R on glass and polypropylene (PP) plates; (d) light transmittance of PAMG-N and PAMG-R viewed under daylight (I, uncovered; II, covered with PAMG-N; III, covered with PAMG-R); (e) macroscopic images of UV shielding (365 nm ultraviolet lamp) by PAMG-N and PAMG-R (I, uncovered 100-yuan banknote; II, 100-yuan banknotes covered with PAMG-N; III, 100-yuan banknotes covered with PAMG-R).

also very obvious (Fig. 6e(II)). The anti-counterfeiting mark covered by PAMG-R, on the other hand, essentially disappeared (Fig. 6e(III)). The ultraviolet shielding performance of the ionogel was further evaluated using commercially available UV test cards (Fig. S4) under both UV lamp and sunlight conditions. PAMG-R exhibited significant UV-blocking efficacy under this assessment.

3.5 Adhesive properties of ionogels

As shown in Fig. 6c, the PAMG-R ionogel shows robust adhesion to glass surfaces, but poor adhesion to polypropylene (PP) surfaces. The strength of bonding of PAMG-R ionogel to common substrate surfaces was quantitatively measured by lap-shear testing. The PAMG-R ionogel achieved a maximum adhesive strength of 139 kPa to glass, whereas its adhesive strength to PP was significantly lower (62.35 kPa). The corresponding tensile strength for PAMG-R adhering to both glass and PP was 42.5 kPa. This disparity arises primarily from the enhanced cohesive strength within the PAMG-R ionogel, which is imparted by chemical bonds and non-covalent interactions within the polymer network. Hydrogen bonds, formed between amino groups on the polyacrylamide molecular side chains of PAMG-R and hydroxyl groups on the glass surface, generate strong interfacial interactions. Adhesion samples prepared on glass substrates and stored at room temperature for 7 days were also evaluated (Fig. S3). The adhesive strength remained stable, without significant fluctuations compared with initial measurements, confirming the sustained adhesive performance of PAMG-R on glass substrates.

4 Conclusion

In this study, PAMG-R ionogels were successfully prepared from rutin, a biomass-derived polyphenol, which was modified by esterification for use as a cross-linking agent. Response surface methodology was used to determine the order of influence of factors on the tensile strength of the ionogels. The optimal ratio of monomers was determined to be: mass fraction of monomer, 36.014%; mass fraction of cross-linking agent, 0.58%; and mass fraction of initiator, 3.714%. Compared with PAMG-N, PAMG-R has greater tensile strength and toughness, together with good compressive properties and toughness. PAMG-R ionogel also has excellent UV-blocking properties and high transparency and shows good adhesion to glass. This study provides a new way to rapidly prepare high-performance UV-resistant polymer coatings, which show promise for use as sunscreen coatings in applications such as parasols and automotive/architectural sunscreen glass.

Author contributions

Dejun Peng: writing, reviewing and editing; writing original draft, methodology, investigation, conceptualization, data curation, funding acquisition, project management. Zeyu Zhang: writing original draft, conceptualization, formal analysis, investigation, methodology. Xueyan Shang: data curation, project management, investigation. Jiguo Zhang: supervision and validation. Shixue Ren: project management, resources, supervision.

Conflicts of interest

The authors declare that they have no known competing financial interests or personal relationships that could have appeared to influence the work reported in this paper.

Data availability

The data supporting this article have been included as part of the SI.

It presents the swelling test results of PAMG-R and PAMG-N, ultraviolet shielding data for esterified rutin, adhesion durability of PAMG-R, and a comparative analysis of its ultraviolet shielding performance against commercial materials. See DOI: **https://doi.org/10.1039/d4lp00381k**.

Acknowledgements

This work was financially supported by the National Training Program of Innovation and Entrepreneurship for Undergraduates (202310225161).

References

1 T. P. Lodge, *Science*, 2008, **321**, 50–51.
2 T. P. Lodge and T. Ueki, *Acc. Chem. Res.*, 2016, **49**, 2107–2114.
3 Y. Ding, J. Zhang, L. Chang, X. Zhang, H. Liu and L. Jiang, *Adv. Mater.*, 2017, **29**, 1704253.
4 L. Shi, K. Jia, Y. Gao, H. Yang, Y. Ma, S. Lu, G. Gao, H. Bu, T. Lu and S. Ding, *Research*, 2020, **2020**, 2505619.
5 R. Tamate, K. Hashimoto, T. Horii, M. Hirasawa, X. Li, M. Shibayama and M. Watanabe, *Adv. Mater.*, 2018, **30**, 1802792.
6 M. Wang, P. Zhang, M. Shamsi, J. L. Thelen, W. Qian, V. K. Truong, J. Ma, J. Hu and M. D. Dickey, *Nat. Mater.*, 2022, **21**, 359–365.
7 N. Chen, H. Zhang, L. Li, R. Chen and S. Guo, *Adv. Energy Mater.*, 2018, **8**, 1702675.
8 Q. Li, Y. Li, D. Hu, X. Liu and Q. Xu, *Chem. Ind. Eng.*, 2023, **40**, 94–104.
9 Y. Hu, MD thesis, *Huazhong University of Science and Technology*, 2023.
10 J. Xu, H. Wang, X. Du and Z. Du, *Polym. Mater.:Sci. Eng.*, 2023, **39**, 138–145.
11 Y. Liu, J. Liu, S. Chen, T. Lei, Y. Kim, S. Niu, H. Wang, X. Wang, A. M. Foudeh, J. B. H. Tok and Z. Bao, *Nat. Biomed. Eng.*, 2019, **3**, 58–68.

12 X. Hu, Y. Cheng, Z. Wei, R. Zhang, Y. Zhan and H. Xia, *ACS Appl. Electron. Mater.*, 2024, **6**, 1770–1780.
13 L. Zheng, J. Wang, R. Lei, W. Chai, H. Jin, H. Ge, X. Wang and D. Jin, *J. China Univ. Metrol.*, 2024, **35**, 152–159.
14 J. Liu, X. Zhang, Y. Cui, Y. Liu, W. Wang, Y. Guo, Q. Wang and X. Dong, *ACS Appl. Mater. Interfaces*, 2024, **16**, 5208–5216.
15 Q. Cui, X. Huang, X. Dong, H. Zhao, X. Liu and X. Zhang, *Chem. Mater.*, 2022, **34**, 10778–10788.
16 Q. Wu, X. Kang, Z. Liu, H. Liu, X. Zhao, T. Liu and Q. Wang, *J. For. Eng.*, 2024, **9**, 87–92.
17 Y. Ren, Z. Liu, G. Jin, M. Yang, Y. Shao, W. Li, Y. Wu, L. Liu and F. Yan, *Adv. Mater.*, 2021, **33**, 2008486.
18 J. Qu, Q. Yuan, Z. Li, Z. Wang, F. Xu, Q. Fan, M. Zhang, X. Qian, X. Wang, X. Wang and M. Xu, *Nano Energy*, 2023, **111**, 108387.
19 M. Wang, J. Hu and M. D. Dickey, *JACS Au*, 2022, **2**, 2645–2657.
20 L. M. Zhang, Y. He, S. Cheng, H. Sheng, K. Dai, W. J. Zheng, M. X. Wang, Z. S. Chen, Y. M. Chen and Z. Suo, *Small*, 2019, **15**, 1804651.
21 S. Hafeez, M. C. Decarli, A. Aldana, M. Ebrahimi, F. A. A. Ruiter, H. Duimel, C. van Blitterswijk, L. M. Pitet, L. Moroni and M. B. Baker, *Adv. Mater.*, 2023, **35**, 2301242.
22 H. C. Yu, H. Zhang, K. Ren, Z. Ying, F. Zhu, J. Qian, J. Ji, Z. L. Wu and Q. Zheng, *ACS Appl. Mater. Interfaces*, 2018, **10**, 9002–9009.
23 G. Guo, J. Sun, Y. Wu, J. Wang, L. Y. Zou, J. J. Huang, K. Ren, C. Liu, Z. L. Wu, Q. Zheng and J. Qian, *J. Mater. Chem. B*, 2022, **10**, 6414–6424.
24 X. Shen, J. L. Shamshina, P. Berton, J. Bandomir, H. Wang, G. Gurau and R. D. Rogers, *ACS Sustainable Chem. Eng.*, 2016, **4**, 471–480.
25 Y. H. Fang, C. Liang, V. Liljeström, Z. P. Lv, O. Ikkala and H. Zhang, *Adv. Mater.*, 2024, **36**, 2402282.
26 Z. Zhang, X. Zhao, X. Song, D. Peng, S. Ren, J. Ren, Y. Ma and S. Li, *Mater. Horiz.*, 2024, **11**, 4171–4182.
27 D. Wu, M. Wang, W. Yu, G. Wang and J. Zhang, *Chem. Eng. J.*, 2024, **486**, 150121.
28 W. Gong, H. B. Huang, X. C. Wang, W. Y. He, Y. Y. Hou and J. N. Hu, *Biomater. Sci.*, 2022, **10**, 6836–6849.
29 L. Dai, M. Ma, J. Xu, C. Si, X. Wang, Z. Liu and Y. Ni, *Chem. Mater.*, 2020, **32**, 4324–4330.
30 D. Gan, W. Xing, L. Jiang, J. Fang, C. Zhao, F. Ren, L. Fang, K. Wang and X. Lu, *Nat. Commun.*, 2019, **10**, 1410–1487.
31 Z. Zhang, D. Peng, X. Shang, X. Zhao, S. Ren, J. Pang and S. Li, *Commun. Mater.*, 2024, **5**, 259.
32 X. Zhao, *Soft Matter*, 2014, **1**, 672–687.
33 K. He, S. Huang, C. Chu and K. Cui, *J. Funct. Polym.*, 2023, **36**, 203–220.
34 T. L. Sun, F. Luo, W. Hong, K. Cui, Y. Huang, H. J. Zhang, D. R. King, T. Kurokawa, T. Nakajima and J. P. Gong, *Macromolecules*, 2017, **50**, 2923–2931.
35 J. Mo, X. Chen, Y. Fu and A. Zhang, *China Elastomerics*, 2019, **29**, 67–75.
36 H. You, S. Zheng, K. Y. Lam and H. Li, *Extreme Mech. Lett.*, 2023, **64**, 102083.
37 M. A. Gwak, B. M. Hong and W. H. Park, *Int. J. Biol. Macromol.*, 2021, **191**, 918–924.
38 K. Fan, K. Li, Z. Yang, Y. Cheng and J. Zhang, *Acta Mater. Compositae Sin.*, 2023, **40**, 3939–3949.